JOURNAL OF SOLID STATE CHEMISTRY 99, 38–51 (1992)

Solid Solution of Metal Oxides in the Zirconolite Phase $CaZrTi_2O_7$. I. Heterotype Solid Solutions

H. J. ROSSELL

C.S.I.R.O. Division of Materials Science and Technology, Locked Bag 33, Clayton 3168, Victoria, Australia

Received September 23, 1991; in revised form December 9, 1991; accepted December 13, 1991

Structure refinement based on powder X-ray diffraction intensities has been carried out on zirconolite phases containing ~10 mole% of various oxides in solid solution. Unambiguous crystallographic location of solute cations was not always possible, but it is shown that the large cations Th^{iv}, Nd^{iii}, Gd^{iii}, Yb^{iii}, and Sc^{iii} substitute for Ca^{ii} and Zr^{iv} in the structure, and that the smaller Fe^{iii}, Co^{ii}, Mg^{ii}, Ta^{v}, and Sn^{iv} substitute for Ti^{iv}, while some exchange of Ti^{iv} and Zr^{iv} also occurs. There is evidence that both cation and anion arrays are intact in these solid solutions, so that the overall stoichiometry is always M_4O_7, i.e., the formal charges of substituting cations are mutually dependent. It is shown that the structure will tolerate substitution of Nd^{iii} or Th^{iv} for Ca^{ii} only if Zr^{iv} is simultaneously substituted by cations of lower charge, e.g., Sc^{iii} or Mg^{ii}: if these are not available, an appropriate amount of Ti^{iii} becomes stabilized in the structure, and this may be supplied from a suitable excess of TiO_2 in the reaction mixture. The extent of the heterotype solid solutions has not been explored: however, in the case of Sn^{iv}, substitution for Ti^{iv} can be complete. Zirconolite-related phases with rhombohedral substructure that form at high solute concentrations are discussed.

Introduction

The titanate ceramic material SYNROC has been designed, on the basis of known geochemistry, to immobilize in solid solution the elements occurring in high-level nuclear wastes with a high degree of assurance, and to form a sufficiently stable solid body for long-term isolation by deep geological burial (*1–6*). SYNROC consists principally of the phases Ba-hollandite ($BaAl_2Ti_6O_{16}$), perovskite ($CaTiO_3$), and zirconolite ($CaZrTi_2O_7$), and is prepared in the form of a dense body by hot pressing suitable mixtures of formant oxides at 1200°C (*6*). Nearly all the fission products, actinides, and processing contaminants in a waste stream can be incorporated at 10–20 wt% in SYNROC at the preparation stage. Various classes of the waste elements distribute preferentially in each of the three phases: in particular, the zirconolite phase incorporates rare-earths and actinides, while Sr and Cs are bound in the perovskite and hollandite, respectively.

The material is considerably more resistant to aqueous leaching than the more popular wasteform of borosilicate glass. Moreover, naturally occurring examples of the relevant phases are known to have retained quantitatively the same chemical elements as those in a waste stream and their daughter products for periods well in excess of the 10^6 years required for safe immobilization, and under accumulated radiation dosages comparable to those expected for SYNROC (*5*).

0022-4596/92 $5.00

There is a large amount of literature concerning the structure and properties of perovskites (*7, 8*), and detailed studies of relevant hollandite phases have been made (*9–11*) which relate structure and chemical properties. The present work is a contribution to the crystal chemistry of the zirconolite phase, which has received comparatively little study.

Natural zirconolite usually is metamict (*12, 13*), but on heating above 1100°C it gradually orders to a fluorite-related superstructure (*14*). The phase $CaZrTi_2O_7$, which can be synthesized readily from the component oxides below ~1500°C (*15*), also has this structure, and it is this ordered form that is termed zirconolite in the discussion below.[1]

The structure of zirconolite has been determined (*18*). It is a C-centered monoclinic fluorite-related superstructure, with axes, referred to the fluorite subcell, of $a = [\bar{1}\bar{1}2]$, $b = [1\bar{1}0]$, $c = \frac{1}{2}[332]$. The supercell thus contains 8 fluorite M_4O_{8-x} subunits. There are crystallographically distinct sites for Ca and Zr, and three Ti sites. The cation ordering is such that alternate planes of metal ions parallel to a set of (111) planes of the basic fluorite substructure essentially contain only Ti and are interleaved by similar planes containing the Ca and Zr arranged in alternating rows. Three-quarters of the Ti cations appear in TiO_6 octahedra linked by corners into a (planar) pattern of six- and three-membered rings similar to that found in the pyrochlore and hexagonal tungsten bronze structures. The remaining Ti occupy randomly one of two sites near the center of a six-ring of TiO_6 octahedra, and are in five-fold coordination by O. The Ca and Zr have respectively eight- and seven-fold coordination by O.

[1] It is recognized that the term "zirkelite" has been recommended (*16*) in place of "zirconolite" for natural material. However, it has been shown (*17*) that zirkelite and zirconolite have a close structural relationship, but nevertheless are quite distinct.

Analyses of synthetic, terrestrial, and lunar zirconolites (*13, 19*) show that four classes of elements can be accommodated in solid solution: (i) Ca, Mg, Fe, Co, and Mn, (ii) Y and rare-earths (*Ln*), (iii) Zr, Hf, U, Th, and Pb, and (iv) Zr, Ti, Nb, Ta, Al, Cr, and perhaps Si. Substitutional solid solution was assumed and assignment of element classes (i) and (ii) to the Ca site, (ii) and (iii) to the Zr site, and (iv) to the Ti sites was made on the basis of known crystal chemistry. In a structure analysis of a terrestrial zirconolite (*20*), the elements present were distributed according to the formula $(Ca_{.85}Ln_{.02}Mn_{.01}Th_{.06}U_{.02})$ $(Zr_{.87}Ti_{.13})$ $(Ti_{.95}Zr_{.13}Nb_{.45}Fe^{ii}_{.12}Fe^{iii}_{.25})O_7$: however, as this assignment did not arise solely by refinement from X-ray diffraction amplitudes but included some subjective judgements, it cannot be regarded as unambiguous. In the present study, further crystal-chemical information on the nature of the solid solutions was sought, and the crystallographic locations of various heterotype solute cations were attempted from measured structure parameters only, using simple synthetic zirconolites.

Experimental

Specimen Preparation

The starting materials were as follows: $CaCO_3$, CoO, Fe_2O_3, MgO, and ThO_2, analytical reagent grade (BDH); ZrO_2, Hf-free grade (Ugine–Kuhlmann); TiO_2, anatase, >99.9% (Fischer); Nd_2O_3, Gd_2O_3, and Yb_2O_3, 99.9% (Atomergic Chemetals); Sc_2O_3, "specpure" (Johnson–Matthey); and Ta_2O_5, optical grade (Nowecki Berylco). The rare-earth and scandium oxides were dissolved in HNO_3, precipitated from acid solution as oxalates, filtered, washed, and calcined to oxides at 1000°C, and the process was repeated in order to remove an unidentified impurity, noticeable particularly in the rare-earth oxides. The $CaCO_3$, ZrO_2, and TiO_2 were subject to atomic ab-

sorption spectroscopic analyses, and were shown to be free of the more probable impurities: in particular, the TiO_2 was shown to contain less than 0.05 mole% of Al_2O_3, a notorious contaminant.

The $CaCO_3$ was dried at 500°C, and all other materials were calcined at 1000°C before use, and stored in a desiccator. The required amounts of these were weighed and ground together under distilled acetone in a boron carbide mortar (preliminary work established that contamination of the starting materials by SiO_2 picked up from an agate mortar led to spurious results). Powders were dried in air, pressed into pellets of ~0.3 g, calcined at 1000°C for 1 hr to decompose the $CaCO_3$ and form $Ca(Ti,Zr)O_3$, then reground and repelleted. These specimens were placed on a Pt sheet in an alumina boat and fired in air at the required temperatures, usually >1300°C, for 4–7 days to form the desired compounds, then quenched in air. The furnace was constructed from alumina refractories with SiC heating elements, and the temperature could be controlled to within ±10°. In a few cases, specimens were fired in flowing N_2 or H_2 and furnace-cooled.

The principal materials so prepared were formulated as follows:

$Ca_{.9}Th_{.1}Ti_{2.2}O_{7+n}$, $Ca_{.9}Th_{.1}Zr_{.9}Mg_{.1}Ti_2O_7$, and $Ca_{.95}Th_{.05}Zr_{.9}Sc_{.1}Ti_2O_7$;

$Ca_{1-x}Nd_{2x}Zr_{1-x}Ti_2O_7$, x = 0.24, 0.20, 0.13, 0.10, 0.05, and 0.025, and $Ca_{.85}Nd_{.15}Zr_{.85}Ti_{2.15}O_{7+n}$;

$Ca_{.88}Gd_{.24}Zr_{.88}Ti_2O_7$ and $Ca_{.8}Yb_{.4}Zr_{.8}Ti_2O_7$, prepared at 1400° C;

$CaZrTi_{1.5}Fe^{iii}_{.25}Ta_{.25}O_7$ and $CaZrTi_{1.5}Co_{.167}Ta_{.333}O_7$, prepared at 1350°C;

$CaZrSn_2O_7$ and $CaZr_{1.24}Sn_{1.76}O_7$, prepared at 1300°C.

Characterization

Lattice parameters were determined by a least-squares procedure from measurement of about 50 diffraction lines on a powder X-ray diffraction pattern recorded with a Guinier camera, using Cu$K\alpha_1$ radiation, and with ThO_2 (a = 5.5972 Å) as an internal standard. Parameters determined for duplicate specimens generally agreed to within twice the estimated standard deviations.

Single-crystal electron diffraction patterns of the specimens, obtained using a 200-kV JEM 200B electron microscope fitted with a tilting stage, were used to confirm the unit cell, and to confirm that, for the solution phases particularly, no defect structures were developed. This technique is the most sensitive for the detection of such phenomena. Some preparations of high Nd content contained a new phase (see below), and these were examined in a JEM 100CX high-resolution electron microscope.

The possible existence of Ti^{iii} in some specimens was investigated by magnetic susceptibility measurements using a Gouy balance, and by the ESCA technique using a Vacuum Generators instrument.

Structure Refinement

Powder X-ray diffraction intensities for $\Theta \leq 40°$ were recorded on a chart, from either a powder diffractometer scanned at 0.25° in 2Θ /min and using Cu$K\alpha_{1,2}$ radiation, or a microdensitometer scanning Guinier films of the specimen (no internal standard). Peak areas were measured with a planimeter and a reflection or group of reflections assigned to each such intensity observation. Reflections indistinguishable from background were assigned an intensity $I_{min}/4$, where I_{min} was the smallest observable intensity, and included in the data. Diffractometer data usually consisted of 250–300 reflections distributed among approximately 120 intensity observations, of which about 20 were of the type $I_{min}/4$, while for Guinier data, the approximate numbers were 400, 200, and 50, respectively.

The larger number of observations that could be obtained from the Guinier films compared to the diffractometer traces was a consequence of the markedly better reso-

lution and the freedom from the complication of $K\alpha_1,\alpha_2$ doublets at high angles. In addition, Guinier data are preferable to diffractometer data because they are not as likely to suffer from preferred orientation effects and are not so critically dependent on particle size in the specimen. However, the precision with which atomic parameters could be determined was not seriously inferior when diffractometer data were used.

Atomic parameters were refined by least-squares from the intensities using POWDER, a computer program appropriate for the treatment of powder data (*21*): the procedure has been described (*22, 23*). The function minimized is $\Sigma w(I_{obs} - I_{calc})^2$, where $w = 1/(I_{obs} + I_{min})$, and the residual quoted is $R = \frac{1}{2}[\Sigma w(I_{obs} - I_{calc})^2/\Sigma w I_{obs}^2]^{1/2}$, which is numerically comparable to the residual commonly quoted for refinements based on single-crystal (F) data. Scattering factors for neutral atoms, with corrections for anomalous dispersion, were taken from the International Tables (*24*).

In each case, a model structure of composition $CaZrTi_2O_7$, with the metal atoms on their ideal sites, and with the published atomic coordinates for this phase (*18, 23*), was assumed, and then the scale factor, the overall isotropic temperature factor, all the variable atomic coordinates, and the occupancies of the metal atom sites were refined. These last quantities allowed a value for the number of electrons, $n(e)$ (i.e., the effective atomic number), at each site to be determined, so that by knowing the composition, an estimate of the most probable metal atom distribution could be made (see below). When possible, the refinement was completed using appropriately combined scattering factors for the metal atoms: $n(e)$ at each site could be determined with an esd of about 0.5. More precise values of $n(e)$ than these are possible, but only if X-ray diffraction data are measured to much higher values of $\sin\Theta/\lambda$ than apply here. This in turn means that only single crystal diffraction data can be used since powder patterns become too confused at large Θ, even for procedures (such as Rietveld profile-fitting) that may use the data more efficiently than that above. Single crystals were not available, and in any case, the values obtained were considered adequate for the present purposes.

The above procedure is based on the assumption that a substitutional solid solution phase occurs in zirconolite in accord with the well-established property of a fully occupied cation sublattice in fluorite-related oxides.

Locating the solute metal atoms from the refinement results is equivalent to finding a distribution of metal atoms in known proportions such that the available sites are filled and at the same time the appropriate values of $n(e)$ at each site are produced within the esd's. If x_{ij} is the fraction of the ith kind of metal atom ($1 \leq i \leq m$, say) at the jth site type ($1 \leq j \leq 5$ for zirconolite), then there are $5m$ unknowns. There are m linear constraint equations of the type $\Sigma_j x_{ij} = p_i$ (from the known stoichiometry) and five each of the types $\Sigma_i x_{ij} = q_j$ (total atoms per site) and $\Sigma_i n(e)_i x_{ij} = n(e)_j$ (as determined): two of these equations are linearly dependent on the others by virtue of the necessary normalizations, leaving $m + 8$ linear equations. In the present cases m is 4 or more, so that there is no unique solution for x_{ij}, but rather a domain of solutions.

The method which was followed is based on a result from linear programming theory; if the domain of the variables is bounded (as it is here), any feasible solution S is a linear combination of basic feasible solutions, $S = \Sigma_i a_i S_i$, where $a_i \geq 0$ and $\Sigma_i a_i = 1$. A basic solution of a set of M linear equations in N unknowns, $N > M$, is a solution obtained by setting $N - M$ unknowns equal to zero and solving for the remaining M unknowns. Not all the apparent solutions (corresponding to all possible distributions of the N–M zeros) exist: for some choices, the $M \times M$

TABLE I

LATTICE PARAMETERS OF VARIOUS SOLID SOLUTION ZIRCONOLITE PHASES

	a, Å	*b*, Å	*c*, Å	ß °
$Ca_{.9}Th_{.1}Zr_{.9}Mg_{.1}Ti_2O_7$	12.4715(9)	7.2684(5)	11.3817(10)	100.539(8)
$Ca_{.95}Th_{.05}Zr_{.9}Sc_{.1}Ti_2O_7$	12.4601(11)	7.2712(6)	11.3863(13)	100.549(8)
$Ca_{.9}Th_{.1}Zr_{.8}Ti^{iii}_{.2}Ti_2O_7$	12.4684(9)	7.2760(5)	11.3628(11)	100.579(8)
$Ca_{.95}Th_{.05}Zr_{.9}Ti^{iii}_{.1}Ti_2O_7$	12.4612(8)	7.2761(5)	11.3778(7)	100.566(6)
$CaTh_{.05}Zr_{.95}Ti_2O_7$ [a]	12.4691(8)	7.2808(5)	11.3996(8)	100.542(7)
$Ca_{.85}Nd_{.15}Zr_{.85}Ti^{iii}_{.15}Ti_2O_7$	12.4862(9)	7.2804(4)	11.3791(7)	100.585(7)
$Ca_{.85}Nd_{.15}Zr_{.85}Sc_{.15}Ti_2O_7$	12.4741(11)	7.2722(6)	11.3899(13)	100.561(9)
$Ca_{.87}Nd_{.26}Zr_{.87}Ti_2O_7$ [a]	12.4997(8)	7.2901(4)	11.4186(9)	100.549(6)
$Ca_{.88}Gd_{.24}Zr_{.88}Ti_2O_7$ [a]	12.4967(11)	7.2863(6)	11.4029(11)	100.563(8)
$Ca_{.8}Yb_{.4}Zr_{.8}Ti_2O_7$	12.4778(8)	7.2673(4)	11.3795(8)	100.550(6)
$CaZrSn_2O_7$ [a]	12.6583(13)	7.4288(8)	11.8280(14)	100.066(9)
$CaZr_{1.24}Sn_{1.76}O_7$	12.6594(14)	7.4227(7)	11.8357(13)	100.065(9)
$CaZrTi_{1.5}Fe_{.25}Ta_{.25}O_7$	12.4826(8)	7.2826(5)	11.4169(9)	100.550(6)
$CaZrTi_{1.5}Co_{.167}Ta_{.333}O_7$	12.4979(8)	7.2906(4)	11.4397(7)	100.493(6)

Note. Numbers in parentheses are esd's and apply to the last quoted places.

[a] Materials of these compositions are not single phases: parameters of the zirconolite phase present are quoted.

matrix of coefficients may be singular; for others, the solution may not be feasible since it contains negative values. Also, it could be seen by inspection in the present cases that many of the unknowns could not be zero. When this procedure was applied to the results from the specimens containing only Ca, Zr, and Ti (see Part II), the only feasible solutions were those representing structures that contained no Ca in any of the Ti sites, a result in accord with crystal-chemical principles. This result therefore was applied as a simplifying assumption in obtaining the domain of solutions for the materials here.

Results and Discussion

The lattice parameters determined for the various phases are given in Table I and the results from the structure refinements in Table II. The basic feasible solutions for site occupancies are given in Table III: those that are considered to be less likely, on the grounds of incompatible ionic radii (*25*) or serious deviation from the Ca/Zr occupancies found in the ternary zirconolites (*18*), have been indicated. Extensive analyses in terms of esd's of individual site occupancies were not made: these values would be 0.02–0.03, but in many cases, linear combinations of probable solutions would cover a

TABLE II

Atomic Coordinates for Various Zirconolite Phases

$Ca_{.9}Th_{.1}Zr_{.9}Mg_{.1}Ti_2O_7$ R = 0.066 N_{obs} = 212

site	n(e)	x	y	z
M1	26.8(4)	.3722(9)	.119(1)	.4957(8)
M2	38.5(4)	.1212(6)	.1227(9)	.9750(5)
M3	21.8(3)	.248(1)	.130(2)	.747(1)
M4	10.0(3)	.472(3)	.063(3)	.256(4)
M5	10.9(3)	0	.129(3)	¼
O1		.296(3)	.138(6)	.284(3)
O2		.476(4)	.148(6)	.101(3)
O3		.210(4)	.087(5)	.575(3)
O4		.392(3)	.130(7)	.724(3)
O5		.708(4)	.190(5)	.582(4)
O6		.987(4)	.145(5)	.424(3)
O7		.109(4)	.041(5)	.793(3)

$Ca_{.95}Th_{.05}Zr_{.9}Sc_{.1}Ti_2O_7$ R = 0.057 N_{obs} = 206

site	n(e)	x	y	z
M1	22.9(3)	.372(1)	.124(2)	.4953(8)
M2	38.1(4)	.1227(5)	.1213(9)	.9750(5)
M3	22.2(2)	.248(1)	.124(2)	.7474(9)
M4	11.3(3)	.466(2)	.049(2)	.2538(6)
M5	11.3(2)	0	.133(2)	¼
O1		.302(2)	.127(6)	.283(3)
O2		.473(3)	.148(5)	.097(3)
O3		.209(3)	.089(5)	.576(3)
O4		.395(3)	.164(5)	.723(3)
O5		.708(3)	.167(4)	.580(3)
O6		.995(3)	.115(5)	.418(3)
O7		.116(3)	.055(4)	.793(3)

$Ca_{.9}Th_{.1}Zr_{.8}Ti^{iii}_{.2}Ti_2O_7$ R = 0.052 N_{obs} = 197

site	n(e)	x	y	z
M1	23.9(3)	.3740(8)	.127(2)	.4971(7)
M2	38.6(4)	.1228(5)	.124(1)	.9749(4)
M3	22.3(3)	.2488(9)	.122(2)	.7474(8)
M4	11.2(4)	.461(2)	.061(2)	.251(3)
M5	11.2(2)	0	.128(3)	¼
O1		.308(2)	.133(5)	.288(3)
O2		.469(3)	.139(5)	.098(2)
O3		.207(3)	.089(4)	.573(3)
O4		.398(3)	.155(5)	.723(3)
O5		.708(3)	.174(4)	.583(3)
O6		.989(2)	.121(5)	.418(3)
O7		.112(3)	.055(4)	.792(3)

$Ca_{.85}Nd_{.15}Zr_{.85}Ti^{iii}_{.15}Ti_2O_7$ R = 0.043 N_{obs} = 122

site	n(e)	x	y	z
M1	24.5(4)	.372(2)	.128(2)	.494(1)
M2	38.3(5)	.119(1)	.125(1)	.9747(7)
M3	22.2(3)	.246(2)	.120(3)	.747(1)
M4	11.0(3)	.470(4)	.053(4)	.260(5)
M5	11.1(3)	0	.125(4)	¼
O1		.320(6)	.115(8)	.273(4)
O2		.474(5)	.118(6)	.102(4)
O3		.202(5)	.099(6)	.580(4)
O4		.380(5)	.169(7)	.716(4)
O5		.731(4)	.152(6)	.588(4)
O6		.979(5)	.157(7)	.406(5)
O7		.100(5)	.047(7)	.801(4)

$Ca_{.88}Gd_{.24}Zr_{.88}Ti_2O_7$ R = 0.050 N_{obs} = 112

site	n(e)	x	y	z
M1	25.4(5)	.378(1)	.125(5)	.499(1)
M2	41.0(4)	.126(1)	.120(2)	.973(1)
M3	23.1(5)	.255(2)	.129(4)	.748(1)
M4	10.5(5)	.468(5)	.062(5)	.233(9)
M5	11.4(3)	0	.115(6)	¼
O1		.331(6)	.114(11)	.319(5)
O2		.468(6)	.131(9)	.116(4)
O3		.190(7)	.081(9)	.574(6)
O4		.384(6)	.154(10)	.695(5)
O5		.710(6)	.187(8)	.596(6)
O6		.986(5)	.136(9)	.417(5)
O7		.114(5)	.066(9)	.815(4)

$Ca_{.8}Yb_{.4}Zr_{.8}Ti_2O_7$ R = 0.057 N_{obs} = 126

site	n(e)	x	y	z
M1	29.7(5)	.372(2)	.126(3)	.495(1)
M2	43.7(4)	.121(1)	.122(2)	.975(1)
M3	22.2(4)	.248(2)	.129(5)	.747(2)
M4	10.5(5)	.461(4)	.058(5)	.255(6)
M5	11.1(3)	0	.126(6)	¼
O1		.310(6)	.130(13)	.274(5)
O2		.479(7)	.125(9)	.111(5)
O3		.220(7)	.079(9)	.567(5)
O4		.403(7)	.154(10)	.715(5)
O5		.714(7)	.171(9)	.587(5)
O6		.004(6)	.124(11)	.417(5)
O7		.117(5)	.067(8)	.785(5)

TABLE II—*Continued*

$CaZrTi_{1.5}Co_{.167}Ta_{.333}O_7$ R = 0.047 N_{obs} = 180

site	n(e)	x	y	z
M1	20.3(5)	.374(1)	.125(2)	.4976(9)
M2	39.7(6)	.1199(5)	.1272(8)	.9756(4)
M3	34.2(6)	.2500(6)	.125(1)	.7426(6)
M4	11.6(3)	.472(2)	.071(2)	.249(4)
M5	13.8(3)	0	.136(2)	¼
O1		.313(3)	.130(5)	.284(3)
O2		.471(3)	.150(4)	.094(3)
O3		.209(3)	.079(4)	.569(3)
O4		.403(3)	.161(5)	.712(3)
O5		.716(3)	.180(4)	.588(3)
O6		.992(3)	.111(4)	.419(3)
O7		.117(3)	.053(4)	.796(3)

$CaZrTi_{1.5}Fe_{.25}Ta_{.25}O_7$ R = 0.048 N_{obs} = 181

site	n(e)	x	y	z
M1	20.5(4)	.375(1)	.123(2)	.4962(9)
M2	40.4(4)	.1220(5)	.1245(8)	.9742(4)
M3	31.6(4)	.2500(7)	.125(1)	.7446(6)
M4	11.5(8)	.471(2)	.061(2)	.252(3)
M5	13.0(3)	0	.130(2)	¼
O1		.309(3)	.123(5)	.289(3)
O2		.470(3)	.145(5)	.099(3)
O3		.206(3)	.082(5)	.574(3)
O4		.396(3)	.167(4)	.718(3)
O5		.706(3)	.176(4)	.584(3)
O6		.995(3)	.115(4)	.426(3)
O7		.112(3)	.049(4)	.794(3)

$CaZr_{1.24}Sn_{1.76}O_7$ R = 0.034 N_{obs} = 90

site	n(e)	x	y	z
M1	21.3(5)	.373(3)	.126(4)	.492(3)
M2	39.9(6)	.126(1)	.130(2)	.986(1)
M3	48.5(16)	.249(1)	.115(2)	.744(1)
M4	22.6(8)	.487(5)	.091(3)	.253(7)
M5	25.0(8)	0	.136(3)	¼
O1		.319(8)	.147(13)	.294(7)
O2		.462(7)	.137(12)	.076(7)
O3		.189(7)	.080(10)	.571(6)
O4		.394(6)	.114(13)	.719(8)
O5		.703(8)	.183(13)	.578(7)
O6		.012(8)	.112(10)	.424(7)
O7		.112(8)	.062(10)	.817(7)

Note. Space group *C2/c* (*27*). Metal atom sites M1 and M2 are the formal "Ca" and "Zr" sites, respectively; M3, M4, and M5 are the "Ti" sites. All sites have occupancy 1.0 atoms except M4 and M5, which are 0.5 atoms: M4 is the "split-atom" site, and M5 is on a diad. Numbers in parentheses are esd's and apply to the last quoted places.

greater range than this. The similarity in the scattering factors of Sc and Ti did not allow these elements to be distinguished formally on the basis of the refinement results. The assignment Ti, Sc in Table III reflects this fact, while the confinement of Sc to sites M1 and M2 is based on the observation that in fluorite-related oxides, the crystal-chemical behavior of Sc is closer to that of Zr rather than that of Ti.

From Table III it can be seen that cation substitution is in accord with crystal–chemical expectations; cations of relatively large radius (Th^{iv}, Nd^{iii}, Gd^{iii}, and perhaps Sc^{iii}) substitute for the eight-coordinated Ca^{ii} and the seven-coordinated Zr^{iv}, while the smaller cations Mg^{ii}, Fe^{iii}, Co^{ii}, Sn^{iv}, and Ta^{v}, which are known to prefer octahedral coordination by O, substitute for Ti^{iv}.

The electron diffraction patterns and elec-

TABLE III

BASIC FEASIBLE SOLUTIONS FOR ATOMIC POPULATIONS IN ZIRCONOLITES

$Ca_{.9}Th_{.1}Zr_{.9}Mg_{.1}Ti_2O_7$

Site	n(g)	Ca	Th	Zr	Mg	Ti	Ca	Th	Zr	Mg	Ti
M1	26.8(4)	.9	.1				.67		.33		
M2	38.5(4)			.9		.1	.23	.1	.57		.1
M3	21.8(3)					1.0					1.0
M4	10.0(3)				.1	.4				.1	.4
M5	10.9(3)					.5					.5

$Ca_{.95}Th_{.05}Zr_{.9}Sc_{.1}Ti_2O_7$

Site	n(g)	Ca	Th	Zr	Sc,Ti	Ti	Ca	Th	Zr	Sc,Ti	Ti	Ca	Th	Zr	Sc,Ti	Ti
M1	22.9(3)	.95	.03	.02			.95	.04		.01		.87		.13		
M2	38.1(4)		.02	.82	.16			.01	.86	.13		.08	.05	.72	.15	
M3	22.2(4)			.06	.94				.04	.96				.05	.95	
M4	11.3(3)					.5					.5					.5
M5	11.3(2)					.5					.5					.5

$CaZrTi_{1.5}Fe_{.25}Ta_{.25}O_7$

Site	n(g)	Ca	Zr	Ti	Fe	Ta	Ca	Zr	Ti	Fe	Ta	Ca	Zr	Ti	Fe	Ta	Ca	Zr	Ti	Fe	Ta
M1	20.5(4)	1.0					1.0					1.0					1.0				
M2	40.4(4)		1.0					1.0					1.0					1.0			
M3	31.6(4)			.79		.21			.79		.21			.69	.10	.21			.55	.25	.20
M4	11.5(3)			.49		.01			.35	.15				.35	.15				.49		.01
M5	13.0(3)			.22	.25	.03			.36	.10	.04			.46		.04			.46		.04

$CaZrTi_{1.5}Co_{.167}Ta_{.333}O_7$

Site	n(g)	Ca	Zr	Ti	Co	Ta	Ca	Zr	Ti	Co	Ta	Ca	Zr	Ti	Co	Ta
M1	20.3(5)	1.0					1.0					1.0				
M2	39.7(6)		1.0					1.0					1.0			
M3	34.2(6)			.72	.01	.27			.73		.27			.57	.17	.26
M4	11.6(3)			.34	.16				.49		.01			.49		.01
M5	13.8(3)			.44		.06			.28	.17	.05			.44		.06

$Ca_{.9}Th_{.1}Zr_{.8}\overset{iii}{Ti}_2\overset{iv}{Ti}_2O_7$

Site	n(g)	Ca	Th	Zr	Ti	Ca	Th	Zr	Ti	Ca	Th	Zr	Ti	Ca	Th	Zr	Ti
M1	23.9(3)	.9	.04	.06		.9	.06		.04	.8		.2		.62		.18	.2
M2	38.6(4)		.06	.74	.2		.04	.8	.16	.1	.1	.6	.2	.28	.1	.62	
M3	22.3(3)				1.0				1.0				1.0				1.0
M4	11.2(4)				.5				.5				.5				.5
M5	11.2(2)				.5				.5				.5				.5

TABLE III—*Continued*

$Ca_{.85}Nd_{.15}Zr_{.85}Ti^{iii}_{.15}Ti^{iv}_{1}O_7$

Site	n(g)	Ca	Nd	Zr	Ti	Ca	Nd	Zr	Ti
M1	24.5(4)	.85	.075	.075		.82	.1	.03	.05
M2	38.3(5)		.075	.775	.15	.03	.05	.82	.10
M3	22.2(3)				1.0				1.0
M4	11.0(3)				.5				.5
M5	11.1(3)				.5				.5

$Ca_{.88}Gd_{.24}Zr_{.88}Ti_2O_7$

Site	n(g)	Ca	Gd	Zr	Ti
M1	25.4(5)	.84	.12	.04	
M2	41.0(4)	.04	.12	.79	.05
M3	23.1(5)			.05	.95
M4	10.5(4)				.5
M5	11.4(3)				.5

$Ca_{.8}Yb_{.4}Zr_{.8}Ti_2O_7$

Site	n(g)	Ca	Yb	Zr	Ti	Ca	Yb	Zr	Ti
M1	29.7(5)	.78	.22			.52		.48	
M2	43.7(5)	.02	.18	.80		.28	.40	.32	
M3	21.2(4)				1.0				1.0
M4	10.5(4)				.5				.5
M5	11.1(3)				.5				.5

$CaZr_{1.24}Sn_{1.76}O_7$

Site	n(g)	Ca	Zr	Sn
M1	21.3(5)	.95	.05	
M2	40.3(6)	.05	.83	.12
M3	49.0(16)		.13	.87
M4	22.8(8)		.23	.27
M5	25.2(8)			.5

Note. Solutions which are considered unlikely for various crystal-chemical reasons have been shaded.

tron micrographs obtained from both the ternary and the solid solution zirconolites showed no evidence for the formation of any serious defects such as fine-scale twins or intergrowths within single crystal fragments. Also, differential electron-density syntheses in both the present and the previous (*18*) X-ray structure studies, as well as the structure refinement results, indicated that the materials basically possessed an intact cation substructure, and that similarly there were no vacancies or interstitials in the anion array. The conclusion that these zirconolites are largely defect-free and that the solute cations are incorporated substitutionally in a structure of constant overall composition, M_4O_7, is compatible with the observation that zirconolites in general are chemically inert. Some further aspects of this appear when the individual solid solution zirconolites are examined in more detail.

The extent of solid solution of the heterotype oxides in zirconolite was not determined per se, as such a study was considered to be a major but separate undertaking. However, some information concerning solid solubilities was obtained here. Initially, materials of the formulation $Ca_{1-x}Ln_{2x}Zr_{1-x}Ti_2O_7$, Ln = Nd, Gd, or Yb, and $x = 0.2$, were prepared on the assumption that $2Ln^{iii}$ would substitute for $Ca^{ii} + Zr^{iv}$ in zirconolite. The material with Ln = Yb and $x = 0.2$ was a single phase, but materials with Ln = Gd or Nd and $x = 0.2$ were a mixture of the zirconolite phase with perovskite and a new hexagonal phase that is described more fully below. The proportion of these extra phases decreased as x was decreased. The hexagonal phase could not be detected when x was less than about 0.15. For Ln = Gd, only a trace of perovskite could be detected in the X-ray powder patterns when x was reduced to 0.12, but for Ln = Nd, no single-phase zirconolite of the above formulation could be prepared, even with x as low as 0.025.

The solid-solution behavior of the rare-earths in zirconolite can be correlated with their formal ionic radii. The results show that Yb most probably substitutes equally at the Ca and Zr sites to form quite extensive

solid solutions, and it may be of significance that the sum of the radii (*25*) of Yb^{iii} in eight- and seven-fold coordination (0.985 + 0.925 = 1.91 Å) is very close to the sum of the radii of eight-coordinated Ca^{ii} and seven-coordinated Zr^{iv} (1.12 + 0.78 = 1.90 Å). The radii of Gd^{iii} are approximately 7% larger than those of Yb^{iii}: the substitution of Gd for Ca and Zr in zirconolite is less extensive than that of Yb.

The radii of Nd^{iii} are about 13% larger than those of Yb^{iii}, and are quite close to those of Ca^{ii}. Material of composition $Ca_{1-x}Nd_{2x}Zr_{1-x}Ti_2O_7$, $x \leq 0.13$, consisted of zirconolite and the perovskite $Ca(Zr,Ti)O_3$, and structure refinement of this zirconolite phase was unsatisfactory since it had to be based on diffraction data which contained the pattern of perovskite of uncertain composition and proportion. Nonetheless, results from $Ca_{.87}Nd_{.26}Zr_{.87}Ti_2O_7$ suggested that Nd most probably substituted for Ca only, and that Ti, equal in amount to the Nd, was present at the Zr site. Following this tentative result, materials $Ca_{1-x}Nd_xZr_{1-x}Ti_{2+x}O_{7+x/2}$, $x \leq 0.2$, were prepared, and these turned out to be single phases; data for the material with $x = 0.15$ is shown in Tables II and III.

It is proposed that the extra Ti enters the Zr site of zirconolite as Ti^{iii} for the following reasons:

(a) Single-phase zirconolite containing Nd could be prepared only if extra Ti, equal in amount to the Nd, was added to the reaction mixture. It is necessary that this be incorporated in the zirconolite structure as Ti^{iii} to preserve charge balance, i.e., an overall stoichiometry of M_4O_7.

(b) The radius of Ti^{iii} is 0.81 Å (*25*), so that it is more appropriate than Ti^{iv} (0.61 Å) in a substitution for Zr^{iv} (0.86 Å).

(c) Replacement of the supposed Ti^{iii} by Sc^{iii} (0.885 Å) or by $\frac{1}{2}(Mg^{ii} + Zr^{iv})$ (0.86 Å) also resulted in single-phase zirconolite.

(d) There was no difference in materials $Ca_{1-x}Nd_xZr_{1-x}Ti_{2+x}O_{7+x/2}$ fired in air at 1400°C and those fired in N_2 or H_2 at 1400°C.

The incorporation of Th in zirconolite was found to be very similar to that of Nd.

(a) Materials $Ca \cdot Zr_{1-x}Ti_2O_7$, $x < 0.1$, were not single phases.

(b) Materials of supposed composition $Ca_{1-x}Th_x \cdot Zr_{1-2x}Ti^{iii}_{2x} \cdot Ti_2O_7$ fired in air at 1400°C were single phase zirconolites. Data for the material with $x = 0.1$ are in Tables II and III.

(c) The materials in (b) were violet-grey: trivalent Ti has a violet color.

(d) Colorless single-phase zirconolites could be made if the supposed Ti^{iii} was replaced by an equivalent amount of colorless Sc^{iii} or $\frac{1}{2}(Mg^{ii} + Zr^{iv})$. An example of each of these is in Tables II and III. These color effects were obscured in zirconolites containing Nd, which itself imparts a deep purple color.

(e) There was no difference between materials in (b) fired in air at 1400°C and those fired in N_2 or H_2 at 1400°C, except that the color was darker if neutral or reducing conditions were imposed.

(f) There was evidence that $Ca_{.9}Th_{.1}Zr_{.8}Ti_{2.2}O_7$ decomposed by oxidation after lengthy exposure in the X-ray diffractometer: the specimen became white, and the perovskite phase, not previously present, appeared.

The stability of Ti^{iii} in air at 1400°C in these Nd- or Th-containing zirconolites is not necessarily a problem. It is commonly stated that Ti_3O_5 and Ti_5O_9 begin to oxidize to TiO_2 at about 800°C in air, and many instances are known of the stabilization of ions including Ti^{iii} in otherwise incompatible conditions by the presence of a suitable crystal field.

Since the influence of Ti^{iii} on the incorporation of actinides and large rare-earths into zirconolite is of importance to SYNROC production, where the conditions are made reducing to control the crystal-chemical behavior of Mo and U, some attempts

were made to confirm Ti^{iii} in these zirconolites.

(a) The ESCA technique returned a null result. No peaks ascribable to any form of Ti other than Ti^{iv} were detected, but on the other hand, zirconolites deliberately reduced in H_2 at 1400°C also returned this null result. Procedures such as EPR and ESR, which may have produced more definitive results, were unavailable.

(b) The magnetic susceptibility of $Ca_{.9}Th_{.1}Zr_{.8}Ti_{2.2}O_7$ was measured on a Gouy balance and the paramagnetic effect of the Ti^{iii}, although small, was determinable and appropriate for the formulation $Ca_{.9}Th_{.1} \cdot Zr_{.8}Ti^{iii}_{.2} \cdot Ti^{iv}_2O_7$. This experiment could not be carried out on the Nd-containing zirconolites because of the masking effect of the rare earth. The materials $Ca_{.9}Th_{.1}Zr_{.9}Mg_{.1}Ti_2O_7$ and $CaZrTi_2O_7$ showed no such magnetic effects.

(c) Approximately 5-g quantities of $Ca_{.9}Th_{.1}Zr_{.8}Ti_{2.2}O_{7.1}$ were prepared from the mixed oxides and $CaCO_3$, compacted, calcined in air at 1100°C, and weighed. The compacts were fired in air at 1400°C for 3 days to form the violet single-phase zirconolite, and weighed again. There was a reproducible weight loss of 0.215%, equivalent to 4.29 mole% of the original TiO_2 being reduced to $TiO_{1.5}$ on formation of the zirconolite, a result consistent with an assignment of Ti^{iii} for about half of the Ti at the Zr site in this material (Table III).

The results in Table III show that the relatively small cations Mg^{ii}, Co^{ii}, Fe^{iii}, Sn^{iv}, and Ta^{v} all substitute for Ti^{iv} in the MO_6 octahedral sheets of the zirconolite structure, and it may be expected that close crystal-chemical relatives of these cations would behave similarly. The scattering factors of Co^{ii}, Fe^{iii}, and Ti^{iv} were too close for these cations to be distinguished at specific Ti sites: Ta^{v} and Mg^{ii}, however, could be located with some precision. The substitution of Ti^{iv} by another small cation in zirconolite is not controlled solely by the cationic radius, but there will be effects due to charge if altervalent cations substitute simultaneously at the Ca and Zr sites. Thus the distribution of Th is probably different in the present Th-containing zirconolites, because of the variation in availability, size, and charge of cations that substitute at the Ti sites. This effect will be relevant in SYNROC production, where the zirconolite phase will be formed in the presence of a great variety of candidate solute cations.

The tin zirconolite is interesting. Material formulated as $CaZrSn_2O_7$ and fired at 1300°C for 2 days consisted of the phases zirconolite, cassiterite (SnO_2), and perovskite ($CaSnO_3$). The tin zirconolite phase formed reasonably rapidly, but after heating at 1250°–1300°C for periods in excess of 4 days it gradually decomposed. Structure refinement of the zirconolite phase was carried out using powder X-ray intensities based on a diffractometer trace; the intensities due to the SnO_2 and $CaSnO_3$ phases were determined separately, scaled to the few relevant unambiguous peaks in the specimen pattern, and subtracted from the overall data. The refinement results and the volume fractions of SnO_2 and $CaSnO_3$ (determined from the scaling) indicated that the zirconolite phase had the composition $CaZr_{1.24}Sn_{1.76}O_7$. Material of this composition, fired in air at 1300°C for 3 days, consisted of the zirconolite phase with a trace of $CaSnO_3$. The refinement results in Tables II and III were based on intensity data from this new specimen. As can be seen, Sn accompanied by a substantial amount of Zr has assumed the place of Ti. The site M4 in all the other zirconolites represents two positions approximately 1 Å apart, one of which is occupied at random by a cation in fivefold coordination by O. In the tin zirconolite, these two closely spaced positions have nearly merged to become a single (fully occupied) position on a diad at $(\frac{1}{2}, 0, \frac{1}{4})$, a position of sixfold triangular prismatic coordination by O. It has been shown that the distance separating the M4 positions was inversely related to the radii of the occupying cations in the

case of the ternary zirconolites $CaZr_xTi_{3-x}O_7$ (*18*), so that the merging of such M4 toward a single site may be correlated with the relatively large radius of Sn^{iv}.

Heavily Doped Zirconolites

As noted above, a hexagonal phase coexisted with zirconolite and perovskite in formulations $Ca_{1-x}Ln_{2x}Zr_{1-x}Ti_2O_7$, Ln = Nd or Gd, $x > 0.15$. The proportion of the hexagonal phase increased at the expense of the others as x was increased; material with $x \sim 0.25$ was mainly hexagonal phase with only a trace of perovskite. The Guinier powder X-ray diffraction pattern of this material was relatively simple and had strong lines indicative of a rhombohedrally distorted, fluorite-derived substructure together with a number of fainter lines. All of the pattern except for a few of the very faint lines could be indexed on the basis of a rhombohedral cell, the hexagonal representation of which had lattice parameters a = 3.6137(2), c = 34.411(2) Å. Two of the very faint extra lines could be indexed if the cell was assumed to be trigonal with twice the above a axis: this cell is dimensionally similar to that reported for zirkelite (*17*).

Electron diffraction patterns from this hexagonal phase (Fig. 1) show, however, that its structure is very complex. The patterns contain all the reflections expected for the zirconolite phase except that reflections in alternate rows parallel to c* have been replaced by groups of closely spaced reflections aligned along c*, while diffuse streaks parallel to c* also occur. The corresponding bright-field electron images (not shown) contain fringes of 11 Å spacing normal to [001], corresponding to the periodicity of zirconolite in that direction, crossed by fainter sets of fringes of variable orientation and spacing. The (001) fringes display a doubled periodicity (alternately light–dark) over lamellar regions about four fringes wide in those cases where the corresponding diffraction pattern has a bunching of the diffuse streaks into incipient spots at half the c* spacing of zirconolite (Fig. 1).

A likely interpretation of these effects is that the sequence of (001) planes containing alternately TiO_6 octahedra and (Ca, Zr) cations that obtains in zirconolite is disrupted on a very fine scale and in a nearly regular manner, to produce a crystal composed of thin lamellar intergrowths of twins or zirconolite-related structures. The boundaries between these lamellae must be such that the cation *positions* characteristic of the basis fluorite-related (111) stacking are not disturbed, since the substructure reflections in the diffraction patterns are unchanged. These electron diffraction results are in accord with those obtained in a detailed high-resolution electron microscopical study of various zirconolite phases from SYNROC formulations (*26*), where evidence was obtained for the coherent intergrowth at the unit cell level of various polytypes and twins of zirconolite that form as a result of stacking anomalies parallel to (001).

The above complex electron diffraction effects are not apparent in Guinier X-ray powder patterns, presumably because they are relatively weak. The "hexagonal" phase determined from Guinier patterns therefore represents the average zirconolite-related substructure of this material. Since the lattice metric and the structure of zirconolite are very close to being hexagonal with unique axis normal to (001) (*13*, *26*), it can be seen that a hexagonal substructure could arise easily when zirconolite itself is densely faulted or twinned on (001) in a quasi-regular manner at about the unit cell level. This faulting or twinning must be confined to domains within an apparent single crystal of zirconolite or to discrete crystallites, since according to the X-ray powder diffraction evidence, zirconolite and "hexagonal" phases coexist and behave as equilibrium phases, i.e., their proportions are a function of the overall composition: if the faulting was randomly distributed, it would be ex-

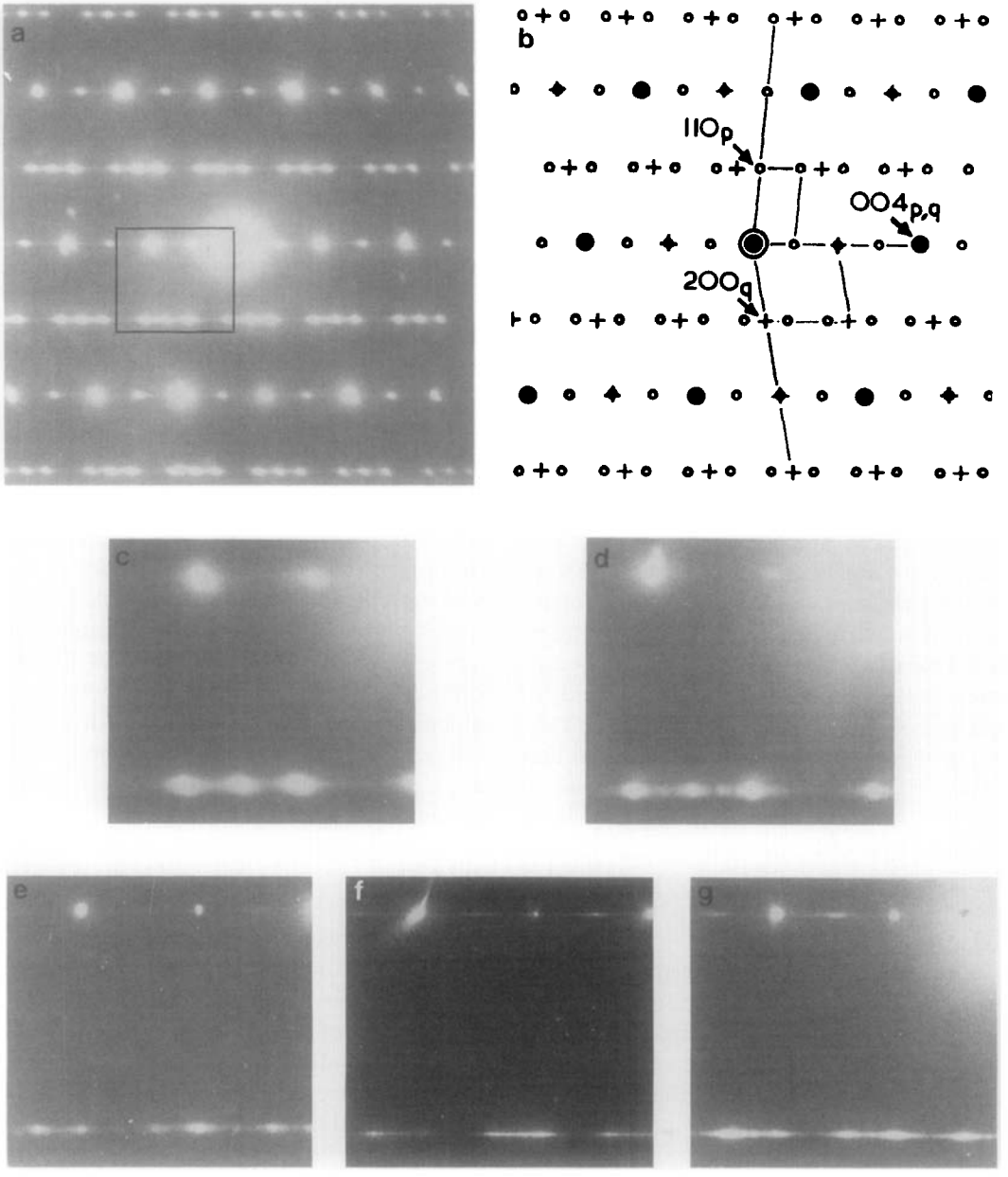

FIG. 1.(a) Electron diffraction pattern from a single crystal fragment of $Ca_{.5}Nd_{.5} \cdot Zr_{.75}Mg_{.25} \cdot Ti_2O_7$. The subcell orientation (fluorite indices) is $[110]_f$. This material is "hexagonal" phase according to the X-ray diffraction data. (b) Demonstration that the pattern in (a) is a superposition of two zirconolite patterns, $p = [1\bar{1}0]$ and $q = [010]$, with common zone c* and coincident (fluorite) substructures (filled spots). In other words, (a) is due to twinned zirconolite. The prominent streaking parallel to c^* in (a) indicates that the twins are very thin (001) lamellae, perhaps 20–30 Å thick. (c) Enlargement of the region outlined in (a). (d)–(g) Regions equivalent to (c) from $[110]_f$ electron diffraction patterns from various other "hexagonal" phases. (d) $Ca_{.5}Nd_{.5} \cdot Zr_{.5}Sc_{.5} \cdot Ti_2O_7$. The similarity with (c) suggests that the crystal is similarly twinned, but the breakup of the streaking into discrete spots suggests a regularity in placement and thickness of the lamellae to give large-scale periodicities. (e) $Ca_{.76}Nd_{.48}Zr_{.76}Ti_2O_7$, (f) and (g) $Ca_{.8}Nd_{.4}Zr_{.8}Ti_2O_7$. The diffraction features are different from those in (c) and (d) so that the above twinning does not apply. The crystals are composed of very thin (001) lamellae of zirconolite-related structures, but of widely differing stacking sequences. In (f) and (g) the c* streaks are bunched into incipient spots, indicating a tendency to a regular repeat at twice the basic zirconolite c* spacing.

pected that the X-ray diffraction pattern of zirconolite would gradually change into that of the "hexagonal" phase as the density of faults increased, and the system would behave as a single phase.

According to the Guinier data, the "hexagonal" phase formed when the preparation of heavily substituted zirconolites was attempted. Thus, $Ca_{.5}Nd_{.5} \cdot Zr_{.5}Sc_{.5} \cdot Ti_2O_7$, $Ca_{.5}Nd_{.5} \cdot Zr_{.75}Mg_{.25} \cdot Ti_2O_7$, and $Ca_{.67}Nd_{.33} \cdot Zr_{.67}Nd_{.33} \cdot Ti_2O_7$ preparations were mainly "hexagonal" phase, while in $Ca_{.33}Nd_{.67} \cdot Zr \cdot Ti_2O_7$, $Nd \cdot Sc \cdot Ti_2O_7$, $Nd \cdot Zr_{.5}Mg_{.5} \cdot Ti_2O_7$, and $Ca_{.7}Th_{.3} \cdot Zr \cdot Ti_{1.7}Co_{.3}O_7$, "hexagonal" and zirconolite phases coexisted. Despite the similarity of the X-ray powder pattern of the "hexagonal" phase in all these materials, the (001) stacking schemes in each case varied considerably in detail, as revealed by electron diffraction (Fig. 1). Further, the variation often seemed to apply to different crystals of a given preparation; see, for example, Figs. 1f and g. Thus, the contention that the formation of densely intergrown twins and polytypes of zirconolite is a mechanism for the incorporation of heterotype solute cations (*26*) is consistent with the results obtained here: it is emphasized, however, that this mechanism would seem to apply only to the more heavily doped zirconolites, as there was no evidence for its occurrence in the zirconolites reported above (Tables I, II, and III).

References

1. A. E. RINGWOOD, S. E. KESSON, N. G. WARE, W. O. HIBBERSON, AND A. MAJOR, *Geochem. J.* **13,** 141 (1979).
2. A. E. RINGWOOD, S. E. KESSON, N. G. WARE, W. O. HIBBERSON, AND A. MAJOR, *Nature* **278,** 219 (1979).
3. K. D. REEVE, D. M. LEVINS, E. J. RAMM, AND J. L. WOOLFREY, "Proceedings, 10th Australian Ceramic Conference," paper 26, p. 143. The Australian Ceramic Soc., Melbourne, 1982.
4. S. E. KESSON, A. E. RINGWOOD, AND R. V. KENT, "Proceedings, 10th Australian Ceramic Conference," The Australian Ceramic Soc., Melbourne, 1982.
5. J. L. WOOLFREY, D. J. CASSIDY, AND K. D. REEVE, "Proceedings 10th Australian Ceramic Conference," The Australian Ceramic Soc., Melbourne, 1982.
6. K. D. REEVE, D. M. LEVINS, E. J. RAMM, J. L. WOOLFREY, AND W. J. BUYKX, *J. Aust. Ceram. Soc.* **18,** 2 (1982).
7. F. S. GALASSO, "Structure, Properties, and Preparation of Perovskite-Type Compounds," Pergamon, Elmsford, NY (1969).
8. N. RAMADASS, *Mater. Sci. Eng.* **36,** 231 (1978).
9. W. SINCLAIR, G. M. MCLAUGHLIN, AND A. E. RINGWOOD, *Acta Crystallogr., Sect. B* **36,** 2913 (1980).
10. L. A. BURSILL AND G. GRZINIC, *Acta Crystallogr., Sect. B* **36,** 2902 (1980).
11. J. E. POST, R. B. VON DREELE, AND P. B. BUSECK, *Acta Crystallogr. Sect. B* **38,** 1056 (1982).
12. L. S. BORODIN, I. I. NAZARENKO, AND T. L. RIKHTER, *Dokl. Akad. Nauk. SSSR* **110,** 845 (1956).
13. Z. V. PUDOVKINA AND YU. A. PYATENKO, *Akad. Sci. USSR Tr.* **17,** 124 (1966).
14. YU. A. PYATENKO AND Z. V. PUDOVKINA, *Kristallografiya* **9,** 98 (1964).
15. L. W. COUGHANOUR, R. S. ROTH, S. MARZULLO, AND F. E. SENNETT, *J. Res. Natl. Bur. Stand.* **54,** 191 (1955).
16. INTERNATIONAL MINERALOGICAL ASSOCIATION: COMMISSION ON NEW MINERALS AND MINERAL NAMES. *Mineral. Mag.* **43,** 1053 (1980).
17. F. MAZZI AND R. MUNNO. *Am. Mineral.* **68,** 262 (1983).
18. B. M. GATEHOUSE, I. E. GREY, R. J. HILL, AND H. J. ROSSELL, *Acta Crystallogr. Sect. B* **37,** 306 (1981).
19. D. A. WARK, A. F. REID, J. F. LOVERING, AND A. EL GORESY. "Abstract, 4th Lunar Science Conference," (J. W. Chamberlain & C. Watkins, Eds.) Houston, March 1973. Pergamon, N.Y.
20. W. SINCLAIR AND R. A. EGGLETON, *Am. Mineral.* **67,** 615 (1982).
21. H. J. ROSSELL AND H. G. SCOTT, *J. Solid State Chem.* **13,** 345 (1975).
22. H. J. ROSSELL, *J. Solid State Chem.* **19,** 103 (1976).
23. H. J. ROSSELL, *Nature* **283,** 282 (1980).
24. "International Tables for X-ray Crystallography," Vol. IV, Tables 2.2A & 2.3.1. Kynoch, Birmingham (1974).
25. R. D. SHANNON, *Acta Crystallogr. Sect. A* **32,** 751 (1976).
26. T. J. WHITE, R. L. SEGALL, J. C. BARRY, AND J. L. HUTCHISON, *Proc. R. Soc. London, A* **392,** 343 (1984).
27. "International Tables for X-ray Crystallography," Vol. I. Kynoch, Birmingham (1969).